RESEARCH PAPER

Design and Fabrication of TiO_2 NP/ NM Nanocomposite as Photoanode for Solar Cells

Rawaa Abbas Abd Ali, Ibrahim Shakir Mutashar, and Majid R. Al-bahrani *

Laboratory of Nanomaterial and Plasma, College of Science, University of Thi-Qar, Thi Qar, Iraq

ARTICLE INFO

Article History:
Received 10 January 2021
Accepted 26 March 2022
Published 01 April 2022

Keywords:
DSSC
Graphene
Hydrothermal
MWCNTs
WS2QD/TiO_2-NC nanocomposite

ABSTRACT

This study presents the preparation of a nanocomposite compound from multi-walled carbon tubes with graphene in a ratio (1:1) and adding it to (TiO_2) and then preparing the resulting compound as photoanode for the DSSC cell after treating it with (WS_2QD) by hydrothermal method and comparing it with the DSSC cell. Based on (TiO_2) as photoanode, the crystal structure of the basic materials and the prepared nanocompositeWS_2QD/ TiO_2-NC have been studied using X-ray diffraction XRD, as well as the SEM and TEM examination. The physical and chemical properties have proved that the nanocomposite (WS_2QD/TiO_2-NC) has been produced within a nanoscale. The regular and pure WS_2QD particles are successfully installed on the nanocomposite TiO_2-NC and exhibit a high surface area and pore size (10μm) when compared to pure WS_2QD. The nanocomposite WS_2QD/TiO_2-NC compound exhibits a PCE conversion efficiency (9.45%), which is relatively high if compared to Pure TiO_2 (8.147%). The reason for improving the PCE of (WS_2QD/TiO_2-NC) is that the presence of MWCNTs and Graphen in the compound reduces the time to reconnect the electron-hole pair and efficiently stabilizes the WS_2QD assembly to expose the entire active edges. On the other hand, giving an increase in electrical conductivity facilitates electron transfer inside the compound. Also, the presence of TiO_2 improves the ability of the compound to absorb the photon and thus increases the photoelectric stimulation.

How to cite this article
Abd Ali R A., Mutashar I S., Al-bahrani M R. Design and Fabrication of TiO_2 NP/ NM Nanocomposite as Photoanode for Solar Cells. J Nanostruct, 2022; 12(2):366-374. DOI: 10.22052/JNS.2022.02.013

INTRODUCTION

The dye-sensitized solar cell technology got piqued the concern of scientists and the public because of its broad range of usage, easiness to manufacture, and high efficiency and longevity. Its system has a sandwich structure that is composed of a semiconductor nanolayer (TiO_2), a dye sensitizer (non-organic, organic, and natural compounds, the commonly used one in the N719 dye is dependent on ruthenium), an electrolyte (iodide/triiodide carrier), as well as a catalyst (basically platinum) coated by conducting substrates (FTO coated glass sheets) [1,2]. It absorbs and is stimulated by sunlight theory. Such electron has been selected through the semiconductor layer because of the preferred energies of its "lower unoccupied molecular orbital" (LUMO). Such electron is transferred into the outer layer by the conducting substratum layer. According to the preferred LUMO energy level, the oxidized (electron-deficient) dye takes an electron from the electrolyte and completes its electrons. The regeneration process begins with the acceptance of an electron from the outer one,

* Corresponding Author Email: *majidphy2016@utq.edu.iq*

reducing the oxidized electrolyte [3,4]. The method of oxidation and regeneration stays reparative till the appearance of light [5,6]. To increase the output of photocurrent and improve the DSSCs efficiency, the light absorption performance of the photoanode, a vital element of DSSCs, has to be improved ultimately. It is estimated that a photoanode with 80 percent absorption of sunlight from 350 to 900 nm will be needed to achieve the power conversion efficiency of more than 15% having I^-/I^{3-} as a redox pair. Polypyridyl ruthenium dyes have a bandgap of 1.8 eV, such as N3 and N719[7,8]. These are currently the most effective traditional sensitizers. As a result, numerous experiments were conducted to improve the photoanodes light-harvesting efficiency without compromising overall performance. Due to their cost-effectiveness, highly stable performance, and excellent electrochemical performance, two-dimensional transition metal chalcogenides (TMDs), which include WS_2, WSe_2, MoS_2 [9-11], $MoSe_2$ [12], and ReS_2 [13], were widely employed as a anode material and in different fields [14,15]. The 2D TMD exhibits uniquely presented electrical and optical properties that are evolved from the quantum confinement and surface effects that are arising through the process of transiting an indirect bandgap to a direct one while scaling down the bulk materials into monolayers. TMDs have a tunable bandgap, heavy photoluminescence (PL), and a high exciton binding energy, getting them a good choice for several optoelectronic devices such as solar cells, photo-detectors, light-emitting diodes, and photo-transistors [16-18].

Because of their tunable bandgap structure, WS2 with a layered structure has got a great interest as a typical material in the set of transitional metals chalcogenides (TMDCs) [19,20]. As the layers are reduced into a single layer, the bandgap is changed into direct. The photoluminescence (PL) strength of monolayer WS2 could be enhanced through 4 orders when compared to multilayer WS2 because of the effects of the quantum confinement in monolayer increasing the likelihood of electrons transitions [21-23], attracting growing attention lie the PL material within the visible and near-infrared ranges [24-26]. Recent studies have shown that WS_2 QDs with very-small sizes (less than 10 nm) have uniquely gathered physical and chemical properties that distinguish them from multilayer and monolayer structures, lie strong PL emission, high PL quantum yields (QY),[27,28] high electroactive sites, huge spin-orbit coupling (420 meV) [29] effect, as well as ultra-small scale. As a result, WS2 QDs have proved that they are excellent for high-efficiency optoelectronic and electrochemical applications. Researchers have recently concentrated on developing low-cost, high-efficiency DSSCs cells, as well as the fabrication of effective optical electrodes and antipodes with high surface stability, reduction catalytic activity, and carbon stability. The fabricated dye-sensitized solar cells system having WS_2/graphene photoanode had an opened circuit voltages (Jsc) of 0.79 mV, a short circuit current (Voc) of 18.6 mA cm^{-2}, a fill factor of 0.66, and a power conversion efficiency of 9.6%, according to A. Prakasam and Krishnamoorthy [30]. M. Durairasan et al. have developed a framework for fabricating tungsten selenide/carbon nanotube (WSe_2/CNT) hybrid photoanodes as potential DSSC anodes. As compared to a pure WSe_2 (86.2 cm2/g and 19.8 nm), WSe_2/CNT hybrid nanostructure has a high surface layer (107.8 cm2/g) and pore size (45.3 nm). The WSe2/CNT composite has a higher photo-conversion efficiency of 8.85%, electrocatalytic activities, and an electron lifetime of 87 nanoseconds [31]. Wu et al. used a hydrothermal method to make a tungsten sulfide/MWCNT hybrid with a presence of glucose to be used as counter electrodes in WS2/MWCNT DSSCs. (Jsc =12.65 mA cm^{-2}, (Voc = 0.73 V), (FF= 0.59), and (percent= 5.45) [32]. MWCNT decorated with WS2 has been synthesized using a hydrothermal process in another study. The material obtained has been used as CE materials to the DSSC, and it has demonstrated the highly catalytic activities to the reducing processes as well as lower charge transferring resistance. A DSSC depending on such counter electrodes has a registered PCE of 6.41 %, which could be compared with the effectiveness of a Pt-based DSSC (6.56 %) [33]. In this paper, a tungsten sulfide / Multi-walled carbon nanotube nanocomposite in the presence of graphene and TiO_2 (WS_2QD / TiO_2-MWCNTs-G) in the presence of glucose has been prepared by the hydrothermal method. The use of nanocomposite as photoanode film material for DSSC, which shows the comparative photoelectric performance of DSSC based on the photoanode TiO_2 film.

MATERIALS AND METHODS

Materials

MWCNTs (95 percent purity), multi-walled

carbon nanotubes with diameters of 8-20 nm and lengths of 5-10 m density: VCN materials (Iran) and graphene with diameters of 20-30 nm yielded 2.1 g/cm^3. N719 (Di-tetrabutylammonium cis-bis (isothiocyanate) bis (2,2′-bipyridyl-4,4′-dicarboxylate) ruthenium has been purchased from Sigma Aldrich (N719 = Di-tetrabutylammonium cis-bis(isothiocyanate) bis (2,2′-bipyridyl-4,4′-dicar (II) 97 percent purity,chemical formula:$C_{58}H_{86}N_8O_8S(2)$ Ru) A fluorine-doped conducting tin oxide SnO_2/F, thickness (2.2 mm), surface resistivity ~7 Ω/cm^{-2}), 77% in the visible range)(FTO) has been obtained from Pilkington TEC Glass. To prepare the (CE) Platinum Wire(diameter: 100 µm) has been used. To prepare the reference DSSCs, commercial TiO_2(Titanium dioxide nanomaterials Density 4.23 g/m^3 at 25C˚), and ethanol (C_2H_5OH) (99.9%) have been used for all experiments and high-purity water. The FTO glass and beakers have been cleaned with ethanol as well as deionized water in an ultrasonication bath for 15 min for each.

Synthesis of WS_2 QD/ TiO_2-NC nanocomposite

Initially, to synthesis, a compound TiO_2-NC mixed with (1:1) Graphen and MWCNTs (NC) with (4 ml) of ethanol and after 10 min of ultrasound stirring, adding (1 g) from TiO_2 to the solution. The solution's PH has been then modified by adding a few drops of acetic acid and stirring for two hours. After we obtained a homogeneous compound solution of nanocomposite TiO_2/ NC. by the used hydrothermal method we added(1g)of tungsten sulfide quantum dot (WS_2 QD) with 50 ml of deionized water to TiO_2 / NC nanocomposite. The as-prepared precursor solution has been put to an autoclave after an hour of ultrasonic stirring and then heated at 160 Co for 72 hours. Being cooled down to room temperature, the suspension has been filtered and cleaned by ethanol several times before being dried at 50 °C.

Fabrication Solar cell device

The three main parts of the DSSC cell sandwich are grouped together. These parts are : Cathode electrode CE prepared in advance by the method of Pt (TEV) on FTO glass plate [34] and photoanode electrode from the nanocomposite WS_2 QD / TiO_2-NC after sintering it on sheets of FTO glass with the doctor blade method, allowing it to dry, and then treating its fixation at 450 °C. The temperature has been raised gradually until it reached 450 Co, and then the sample is immersed after it had been cooled in N719 dye for 24 hours at room temperature,(3) The electrolytic solution(I^- / I^{3-}) was placed between the two electrodes. A Keithley digital controller is used to track the DSSC's current image (J-V) studies (model 2400). The photoelectric output was achieved by the use of a Xenon 500 W optical filter as a solar light source. The electrode material has 1 cm^2 active surface.

Characterization and Measurement

An emission scanning and transmission of electron microscopes (SEM, and TEM) have been employed to test the samples' morphologies. Analyzing the structural properties is an important and essential method for crystalline structure research. X-ray diffraction is commonly used to investigate the structural properties of nanocomposite WS2 QD/TiO2-NC. The above-mentioned solar cell's output can be measured using the cell efficiency (PCE) and fill factor (FF) equations:

$$FF = \frac{V_{max}\ x\ J_{max}}{V_{OC}\ x\ J_{SC}} \quad (1)$$

$$PCE\ (\eta) = \frac{V_{oc}\ x\ J_{SC}\ X\ FF}{Pin}\ x\ 100\% \quad (2)$$

RESULTS AND DISCUSSION

Morphology and Composition: Figure 1a shows an SEM image of the formation of thin films of TiO_2 nanoparticles deposited on FTO and the entire surface appears homogeneously covered with TiO_2 and nanoparticles of an average size of (10µm). The X-ray diffraction (XRD) patterns are illustrated below (Fig. 1d) for the TiO_2 film, which is deposited on the FTO as optical pole peaks with values of 2theta (degree) (24.4° - 101), (37.9° - 004),(48.2° -200), (53.8° -105), (55.1° - 211), (62.9° -204) where large peaks indicate high crystallinity of TiO_2 particles deposited on FTO. This indicates that the TiO_2 optical electrode contains a porous structure with a large surface area that enhances the harvest. Light and absorption of N719 dye electrons.

The J-V curve of the TiO_2 as shown in Fig. 1c was obtained under a simulated 100 mW /cm^2 AM1.5 G solar simulation several solar cell parameters can be deduced as Jsc , Voc and FF see table (1). In the present paper also, the sol-gel methodology was used for preparing (TiO_2/MWCNTs) nanocomposite powder having (0.02 wt %) MWCNTs to be used as

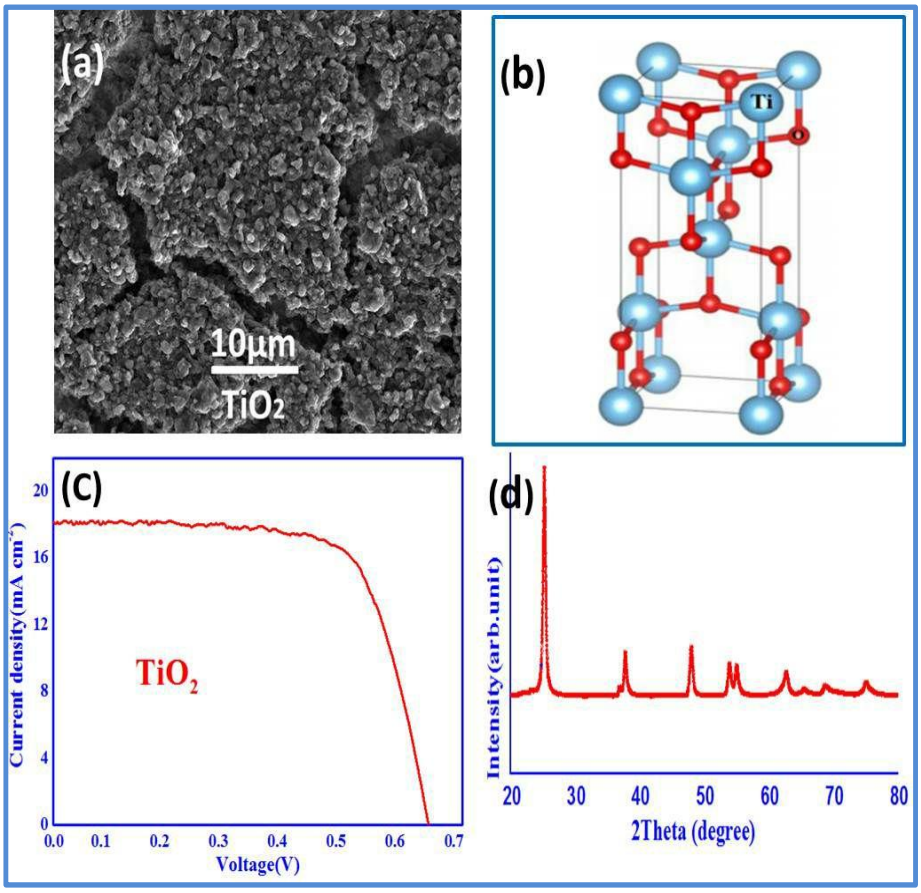

Fig. 1. (a) SEM image of pure TiO_2(b) structures nanoscale of TiO_2 (c) Photocurrent density voltage characteristics of TiO_2 (d) XRD of pure TiO_2 nanoparticles.

a photoanode in dye-sensitized solar cells (DSSCs). Using a doctor-blade process, they have been allocated onto transparent-conducting (FTO) glass substrates and after that stabled with dyes N719. The findings show the ratio of MWCNTs to TiO_2 and the inter-connection of them had a substantial impact on the properties of their structure, optics, and photo-volt. In addition, the assembled DSSCs with counter electrode Pt (TEV) were examined under one sun irradiation (100 mW/cm^{-2}). The incident conversion efficiency of photon-to-current (PCE) and calculated current-voltage (IV)

Table 1. Photovoltaic parameters of TiO_2 pure and nanocomposites samples TiO_2 / MWCNTs, TiO_2/ NC, and WS_2 QD / TiO_2-NC as photoanode in DSSCs.

PE	CE	Jsc(mA/cm^2)	Voc(V)	FF%	PCE%
TiO_2	Pt TEV	17.94	0.664	0.684	8.147
TiO_2/MWCNTs	Pt TEV	18.48	0.665	0.705	8.660
TiO_2/NC	Pt TEV	18.79	0.677	0.705	8.960
WS_2QD/TiO_2-NC	Pt TEV	19.35	0.677	0.722	9.450

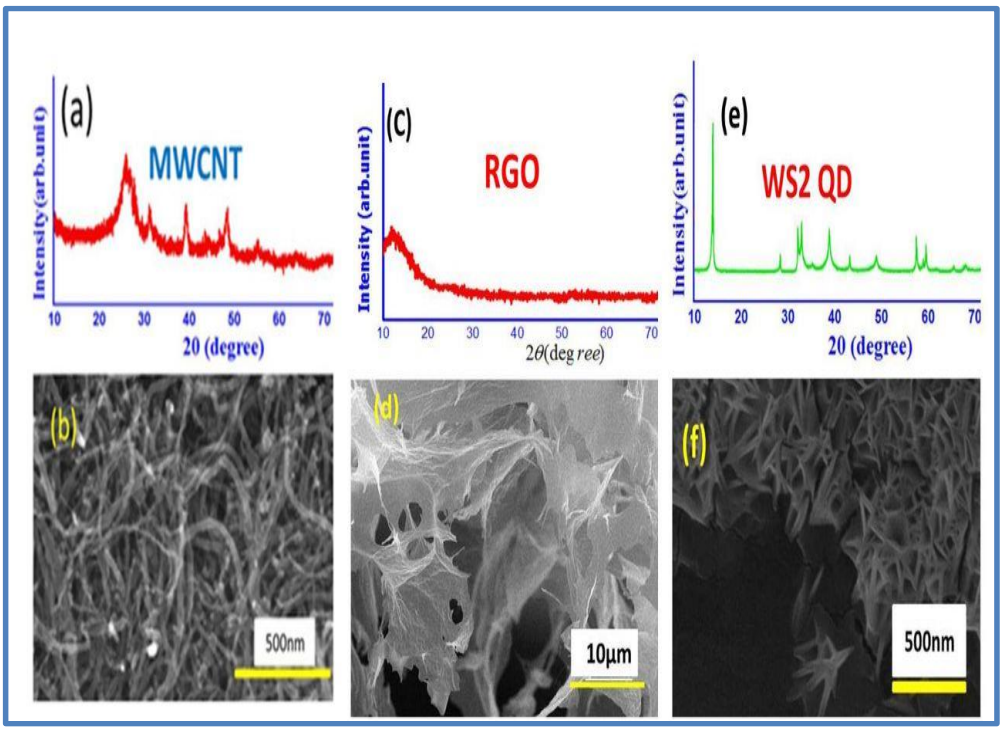

Fig. 2. (a,c,e) XRD of pure MWCNTs, RGO, and WS_2QD nanoparticles respectively (b,d,f) SEM images of pure MWCNTs, RGO, and WS_2QD nanoparticles respectively also.

curve of nanocomposite TiO_2/ MWCNTs are shown in Fig. (4- a) (8.127 %).

When using the hydrothermal method to combine Graphene and MWCNTs at a ratio of 1 percent Graphene/1 percent MWCNTs with TiO_2, the obtained results showed a slight synergistic effect in the NC bi-filler hybrid composites, resulting in higher electrical conductivity and surface area for nanocomposite TiO_2/NC. This improvement was due to the interaction between NC and TiO_2, which limited the graphene aggregation and enabled MWCNTs to bridge adjacent graphene platelets, resulting in higher values of (Jsc = 18.79 mA/cm^{-2}) and (Voc = 0,677 V) comparative than when nanocomposite TiO2/ MWCNTs were present alone, bringing the PCE for the cell to 8.960 %.

Table 1 can explain the fact that MWCNTs can act as an electron bridge in the photoanode of nanocomposite TiO_2 / MWCNTs, transferring electrons to the current collector and reducing recombination in the device. The inclusion of materials (NC) in the photoanode of nanocomposite TiO_2/NC also increases the dye absorption capacity and increases the light harvest ultimately the increase in PCE to 8.960 %. The PCE of the photoanode of nanocomposite TiO_2/NC increased when WS_2 QD was introduced to TiO_2/ NC due to the increase in the absorption surface area and the increase in light harvest because WS_2 QD was in a coating around the compound NC. Consequently, the PCE of the cell with the photoanode nanocomposite WS_2 QD/TiO_2-NC was increased to 9.450%.

Before beginning the fabrication process, morphological studies of the material were carried out, and the results are shown in Fig. 2. The MWCNTs used in the experiment are shown in Fig. 2b. The MWCNTs had an average diameter of 20 nm. Figure 2d shows an SEM picture of prepared RGO, which appears to be a sheet and was hydrothermally broken into small spherical sheets in an alkaline atmosphere, while the WS_2 QD sample showed aggregated spherical morphology (Fig. 2f).

XRD analysis has been adopted for characterizing the microstructure of pure MWCNTs, RGO, and WS_2 QD samples, and the resulting diffraction pattern. (Fig. 2 a,b and c). The XRD pattern of MWCNTs (Fig. 2a) indicates a sharply shaped peak at 26.170 that corresponds with (002) reflections, indicating the existence of elemental carbons (JCPDS No. 41-

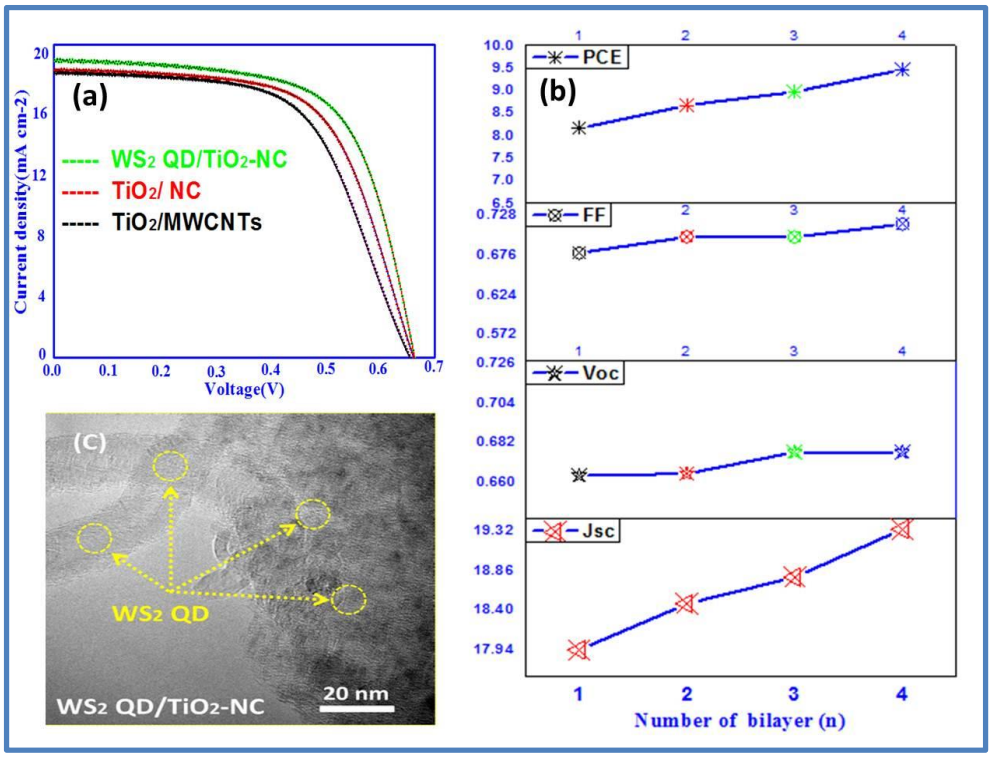

Fig. 3. (a) Photocurrent density voltage characteristics of nanocomposites TiO_2/MWCNTs, TiO_2/NC and WS_2 QD/TiO_2 -NC (b) the described DSSCs can be evaluated in terms of, Fill factor (FF), Jsc, Voc, and cell efficiency (PCE) (c) TEM images of nanocomposite WS_2QD/TiO_2-NC.

1487), and the XRD patterns of RGO are shown in Fig. 2 c. A sharp peak at 2 theta = 10.31o is due to (001) graphene oxide in the spectrum. After the thermal reduction phase, the sample peak shifts to the right side at 2thati = 21o [35]. Furthermore, the RGO interlayer gap decreased as the peak shifted toward a greater angle. As a consequence, Bragg's law (2d sinθ = nλ) applies. Fig. 1(e) demonstrates the hexagonal crystalline nature of WS_2 QDs, having the characterized peaks at 2thati =14.3° for the (002) plane [36]. The peaks with lower intensities of the (002) plane show the process of forming an ultrathin structure of WS_2 QD in comparison with (004) planes of WS2 at 2 theta =27.0°. In addition to the hexagonal plane, the existence of the (006) plane in the XRD patterning indicates the availability of WS_2 rhombohedra structures, as previously reported [37]. Furthermore, the (102) and (106) planes in the XRD patterning have WS_2 contents signatures.

Morphology and compositions of the nanocomposite WS_2 QD/ TiO_2- NC

The SEM image and XRD of the nanocomposite WS_2 QD/ TiO2- NC is illustrated in Fig. 3. The SEM image in (Fig. 3b) illustrates the hydrothermal synthesis of WS_2 QD results in irregular aggregated particles with a coral-like shape, which can provide a broad specific surface area of absorption. The coral-like structure of the WS_2 QD particles can still be seen in the NC hybrid, and they are distributed uniformly. The surface of the nanocomposite WS_2 QD/TiO_2-NC becomes rougher when compared to pristine MWCNTs and graphene (Fig. 2 b,d,f) and TiO_2 in (Fig. 1a), indicating that the WS_2 QD particles are successfully decorated onto the surfaces of the MWCNTs and graphene, similar to how wrinkled graphene sheets were coated onto the surfaces of MWCNTs in NC hybrid.

Fig. 4a shows the diffraction peaks at the highest values which can be assigned as the contribution from the WS_2 QD, and the strongest peak. 4(a) shows the XRD patterns of the nanocomposite WS_2 QD/TiO_2-NC. This demonstrates a lack of crystalline. The XRD pattern of the WS_2 QD/ TiO_2-NC shows all of the MWCNTs, WS_2QD, and TiO_2 characteristic diffraction peaks. This shows that after the hydrothermal phase, WS_2QD particles

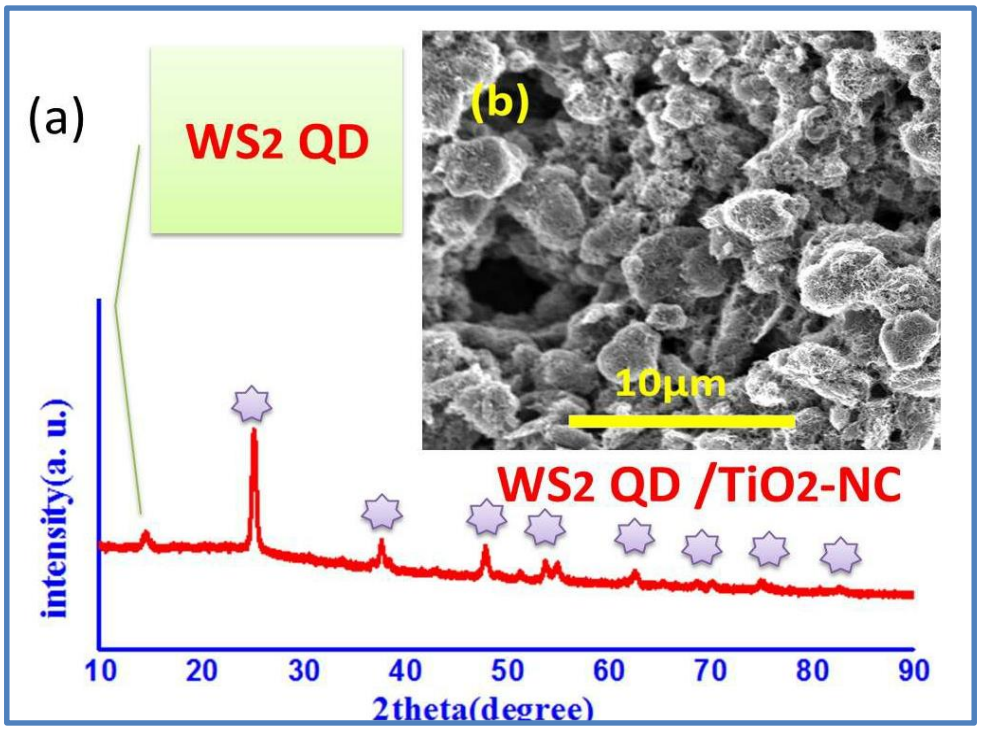

Fig. 4. (a) XRD of nanocomposite WS_2 QD/TiO_2-NC (b) SEM image of WS_2 QD/TiO_2-NC

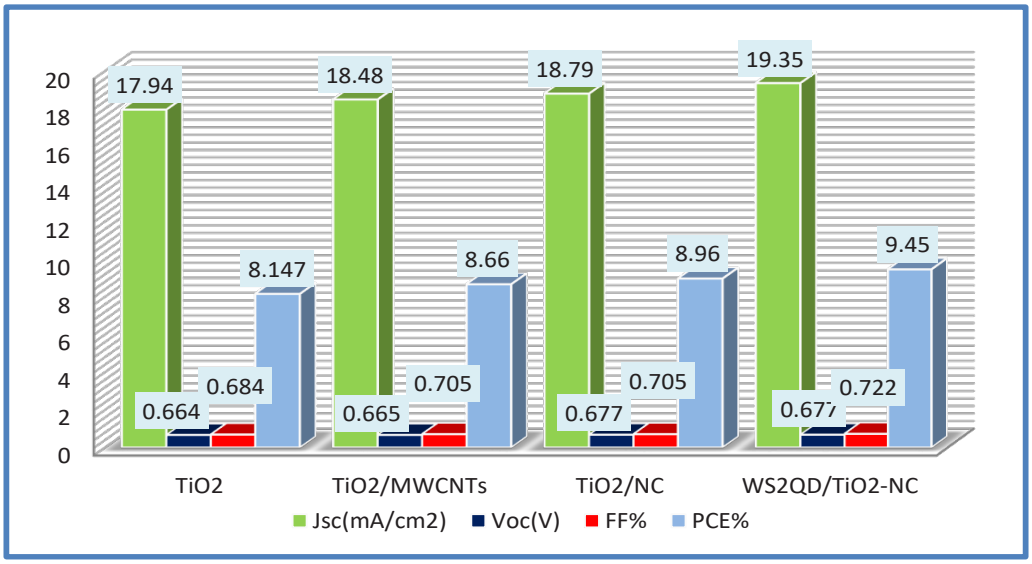

Fig. 5. Devices performance of the DSSCs as a function of Jsc, Voc, Fill Factor FF and Efficiency PCE.

are incorporated into TiO_2-NC. TEM analysis was performed to examine the microstructure of WS_2 QD/ TiO_2- NC in greater detail, as shown in Fig. 3 c. The WS_2 QD nanocrystals have been bound to the surface of the NC hybrid, which is noteworthy. These TEM findings show that WS_2QD nanoparticles are successfully decorated on the NC hybrid surface. The WS_2 QD/TiO_2-NC nanocomposite prepared in this study is highly active catalytically to the absorbing photon processes and a lower resistances for charge transferring. A DSSC based on this photoanode

has a registered PCE of 9.45 % "under simulated solar illumination of 100 mW cm^2", which could be compared with a photoanode TiO_2 DSSC (8.147 %) see Fig. 5. The outstanding performance is due to the fact that the nanocomposite WS_2 QD/TiO_2-NC structure has huge specific surface areas which can be employed in the interfering reactions and has a lot of potentials for improving photovoltaic performance in DSSCs.

The reason for improving the PCE of (WS_2QD/ TiO_2-NC) is that the presence of MWCNTs and Graphen in the compound reduces the time to reconnect the electron-hole pair and efficiently stabilizes the WS_2QD assembly to expose the entire active edges while giving an increase in electrical conductivity that facilitates electron transfer inside the compound. In addition, the presence of TiO_2 improves the ability of the compound to absorb the photon and thus increase the photoelectric stimulation, as well as the nanocomposite crystal structure of WS_2QD /TiO_2-NC which allows effective ionic diffusion and helps in infiltration for (I^- / I^{-3}) easily.

CONCLUSIONS

In short, a simple and safe method for manufacturing a photoanode column using the hydrothermal method using multiple nanomaterials. XRD analysis confirmed the successful synthesis of pure and homogeneous nanocomposite WS_2QD / TiO_2-NC hybrid nanoparticles and retention of the crystal structure. The SEM images revealed a porous morphological structure. We believe that the great improvement in conversion efficiency PCE to(9.45%) of nanocomposite (WS_2QD / TiO_2-NC) results from the good properties of the materials used in terms of high electrical conductivity, large and effective surface area.

CONFLICT OF INTEREST

The authors declare that there is no conflict of interests regarding the publication of this manuscript.

REFERENCE

1. Shakeel Ahmad M, Pandey AK, Abd Rahim N. Advancements in the development of TiO_2 photoanodes and its fabrication methods for dye sensitized solar cell (DSSC) applications. A review. Renewable and Sustainable Energy Reviews. 2017;77:89-108.
2. Ahmad W, Chu L, Al-bahrani MR, Yang Z, Wang S, Li L, et al. Formation of short three dimensional porous assemblies of super hydrophobic acetylene black intertwined by copper oxide nanorods for a robust counter electrode of DSSCs. RSC Advances. 2015;5(45):35635-42.
3. Ahmad MS, Pandey AK, Rahim NA. Effect of Nanodiamonds on the Optoelectronic Properties of TiO_2 Photoanode in Dye-Sensitized Solar Cell. Arabian Journal for Science and Engineering. 2017;43(7):3515-9.
4. Pandey AK, Ahmad MS, Alizadeh M, Rahim NA. Improved electron density through hetero-junction binary sensitized TiO_2/ CdTe / D719 system as photoanode for dye sensitized solar cell. Physica E: Low-dimensional Systems and Nanostructures. 2018;101:139-43.
5. Al-bahrani MR, Ahmad W, Ruan S-S, Yang Z, Cheng Z, Gao Y. Layer-by-layer deposition of CNT and CNT hybrid films for platinum free counters electrodes of dye-sensitized-solar-cells. RSC Advances. 2015;5(116):95551-7.
6. Ahmad MS, Pandey AK, Rahim NA, Shahabuddin S, Tyagi SK. Chemical sintering of TiO_2 based photoanode for efficient dye sensitized solar cells using Zn nanoparticles. Ceram Int. 2018;44(15):18444-9.
7. Zhang X, Zhang J-J, Xia Y-Y. A comparative theoretical investigation of ruthenium dyes in dye-sensitized solar cells. J Photochem Photobiol A: Chem. 2007;185(2-3):283-8.
8. Dell'Orto E, Raimondo L, Sassella A, Abbotto A. Dye-sensitized solar cells: spectroscopic evaluation of dye loading on TiO_2. J Mater Chem. 2012;22(22):11364.
9. Liu Y, Wang W, Huang H, Gu L, Wang Y, Peng X. The highly enhanced performance of lamellar WS_2 nanosheet electrodes upon intercalation of single-walled carbon nanotubes for supercapacitors and lithium ions batteries. Chem Commun. 2014;50(34):4485.
10. Chen F, Wang J, Li B, Yao C, Bao H, Shi Y. Nanocasting synthesis of ordered mesoporous crystalline WSe_2 as anode material for Li-ion batteries. Mater Lett. 2014;136:191-4.
11. Yu X-Y, Hu H, Wang Y, Chen H, Lou XWD. Ultrathin MoS_2Nanosheets Supported on N-doped Carbon Nanoboxes with Enhanced Lithium Storage and Electrocatalytic Properties. Angew Chem. 2015;127(25):7503-6.
12. Zheng C, Chen C, Chen L, Wei M. A CMK-5-encapsulated $MoSe_2$ composite for rechargeable lithium-ion batteries with improved electrochemical performance. Journal of Materials Chemistry A. 2017;5(37):19632-8.
13. Qi F, Chen Y, Zheng B, He J, Li Q, Wang X, et al. 3D chrysanthemum-like ReS_2 microspheres composed of curly few-layered nanosheets with enhanced electrochemical properties for lithium-ion batteries. Journal of Materials Science. 2016;52(7):3622-9.
14. Wang Z, Li Q, Xu H, Dahl-Petersen C, Yang Q, Cheng D, et al. Controllable etching of MoS_2 basal planes for enhanced hydrogen evolution through the formation of active edge sites. Nano Energy. 2018;49:634-43.
15. Wang Z, Li Q, Besenbacher F, Dong M. Facile Synthesis of Single Crystal $PtSe_2$ Nanosheets for Nanoscale Electronics. Adv Mater. 2016;28(46):10224-9.
16. Bao W, Cai X, Kim D, Sridhara K, Fuhrer MS. High mobility ambipolar MoS_2 field-effect transistors: Substrate and dielectric effects. Appl Phys Lett. 2013;102(4):042104.
17. Islam MR, Kang N, Bhanu U, Paudel HP, Erementchouk M, Tetard L, et al. Tuning the electrical property via defect engineering of single layer MoS_2 by oxygen plasma. Nanoscale. 2014;6(17):10033-9.
18. Bhandavat R, David L, Singh G. Synthesis of Surface-

Functionalized WS_2 Nanosheets and Performance as Li-Ion Battery Anodes. The Journal of Physical Chemistry Letters. 2012;3(11):1523-30.
19. Wang QH, Kalantar-Zadeh K, Kis A, Coleman JN, Strano MS. Electronics and optoelectronics of two-dimensional transition metal dichalcogenides. Nature Nanotechnology. 2012;7(11):699-712.
20. Wu W, Wang L, Li Y, Zhang F, Lin L, Niu S, et al. Piezoelectricity of single-atomic-layer MoS_2 for energy conversion and piezotronics. Nature. 2014;514(7523):470-4.
21. Zhao W, Ghorannevis Z, Chu L, Toh M, Kloc C, Tan P-H, et al. Evolution of Electronic Structure in Atomically Thin Sheets of WS_2 and WSe_2. ACS Nano. 2012;7(1):791-7.
22. Gutiérrez HR, Perea-López N, Elías AL, Berkdemir A, Wang B, Lv R, et al. Extraordinary Room-Temperature Photoluminescence in Triangular WS_2 Monolayers. Nano Lett. 2012;13(8):3447-54.
23. Sweet C, Pramanik A, Jones S, Ray PC. Two-Photon Fluorescent Molybdenum Disulfide Dots for Targeted Prostate Cancer Imaging in the Biological II Window. ACS Omega. 2017;2(5):1826-35.
24. Elías AL, Perea-López N, Castro-Beltrán A, Berkdemir A, Lv R, Feng S, et al. Controlled Synthesis and Transfer of Large-Area WS_2 Sheets: From Single Layer to Few Layers. ACS Nano. 2013;7(6):5235-42.
25. Zhang S, Dong N, McEvoy N, O'Brien M, Winters S, Berner NC, et al. Direct Observation of Degenerate Two-Photon Absorption and Its Saturation in WS_2 and MoS_2 Monolayer and Few-Layer Films. ACS Nano. 2015;9(7):7142-50.
26. Peimyoo N, Shang J, Cong C, Shen X, Wu X, Yeow EKL, et al. Nonblinking, Intense Two-Dimensional Light Emitter: Monolayer WS_2 Triangles. ACS Nano. 2013;7(12):10985-94.
27. Ye Z, Cao T, O'Brien K, Zhu H, Yin X, Wang Y, et al. Probing excitonic dark states in single-layer tungsten disulphide. Nature. 2014;513(7517):214-8.
28. Lin L, Xu Y, Zhang S, Ross IM, Ong ACM, Allwood DA. Fabrication of Luminescent Monolayered Tungsten Dichalcogenides Quantum Dots with Giant Spin-Valley Coupling. ACS Nano. 2013;7(9):8214-23.
29. Krishnamoorthy D, Prakasam A. Graphene Hybridized with Tungsten disulfide (WS_2) Based Heterojunctions Photoanode Materials for High Performance Dye Sensitized Solar Cell Device (DSSCs) Applications. J Cluster Sci. 2020;32(3):621-30.
30. Durairasan M, Karthik PS, Balaji J, Rajeshkanna B. Design and fabrication of WSe_2/CNTs hybrid network: A highly efficient and stable electrodes for dye sensitized solar cells (DSSCs). Diamond Relat Mater. 2021;111:108174.
31. Wu J, Yue G, Xiao Y, Huang M, Lin J, Fan L, et al. Glucose Aided Preparation of Tungsten Sulfide/Multi-Wall Carbon Nanotube Hybrid and Use as Counter Electrode in Dye-Sensitized Solar Cells. ACS Applied Materials & Interfaces. 2012;4(12):6530-6.
32. Yue G, Wu J, Lin J-Y, Xiao Y, Tai S-Y, Lin J, et al. A counter electrode of multi-wall carbon nanotubes decorated with tungsten sulfide used in dye-sensitized solar cells. Carbon. 2013;55:1-9.
33. Zhao C, Xing L, Xiang J, Cui L, Jiao J, Sai H, et al. Formation of uniform reduced graphene oxide films on modified PET substrates using drop-casting method. Particuology. 2014;17:66-73.
34. Sawant JP, Kale RB. CZTS counter electrode in dye-sensitized solar cell: enhancement in photo conversion efficiency with morphology of TiO_2 nanostructured thin films. J Solid State Electrochem. 2019;24(2):461-72.
35. Huízar-Félix AM, Cruz-Silva R, Barandiarán JM, García-Gutiérrez DI, Orue I, Merida D, et al. Magnetic properties of thermally reduced graphene oxide decorated with PtNi nanoparticles. J Alloys Compd. 2016;678:541-8.
36. Ghorai A, Midya A, Ray SK. Superior charge storage performance of WS_2 quantum dots in a flexible solid state supercapacitor. New J Chem. 2018;42(5):3609-13.
37. Sharma S, Bhagat S, Singh J, Singh RC, Sharma S. Excitation-dependent photoluminescence from WS_2 nanostructures synthesized via top-down approach. Journal of Materials Science. 2017;52(19):11326-36.